ACS APPLIED MATERIALS & INTERFACES

Research Article

www.acsami.org

Cyclometalated Ruthenium Sensitizers Bearing a Triphenylamino Group for p-Type NiO Dye-Sensitized Solar Cells

Zhiqiang Ji, Gaytri Natu, and Yiying Wu*

Department of Chemistry & Biochemistry, The Ohio State University, 100 West 18th Avenue, Columbus, Ohio 43210, United States

Supporting Information

ABSTRACT: We report the synthesis, photophysical, and electrochemical studies of a series of cyclometalated ruthenium sensitizers carrying triphenylamino linkers for p-type NiO dye-sensitized solar cells (DSSCs). The general structure of these ruthenium sensitizers is Ru[N^N]$_2$[N^C], where [N^N] is a diimine ligand and [N^C] is a cyclometalated ligand. The triphenylamino group is attached to the *-para* position of the ruthenium−carbon bond of the [N^C] ligand as a linker to bridge the ruthenium chromophore and the NiO surface and to enhance the electronic coupling for hole injection. As a result, cells made with these sensitizers generate higher short-circuit currents (J_{sc}) than cells sensitized with our prior sensitizers with phenylene linkers. Morever the N^N ligands are systematically tuned from 2,2′-bipyridine (**O3**), to 1,10-phenanthroline (**O13**), and to bathophenanthroline (**O17**). Following the series, the conjugation of the NN ligand is increased, which results in the enhancement of extinction coefficient and the red shift of light absorption. However the solar cell sensitized with **O3** still gives the largest J_{sc} of 3.04 mA/cm^2. The large J_{sc} highlights the promising potential of using these cyclometalated ruthenium sensitizers for NiO DSSCs. In addition, the carrier dynamics of these solar cells has been systematically studied by intensity-modulated photovoltage spectroscopy (IMVS) and intensity-modulated photocurrent spectroscopy (IMPS). The results suggest that the **O3** solar cell giving the largest J_{sc} is likely caused by the slow geminate charge recombination and efficient dye regeneration.

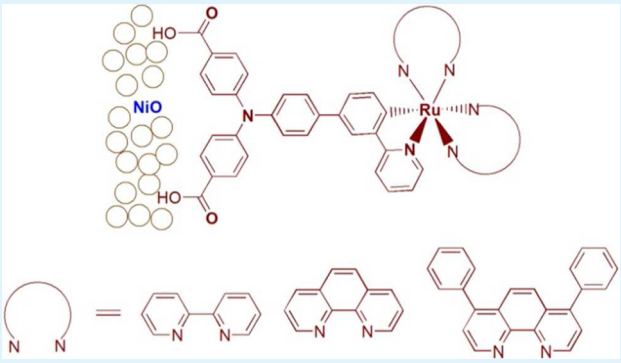

KEYWORDS: *p-type dye-sensitized solar cell, NiO, cylcometalated ruthenium sensitizer, triphenylamino group*

INTRODUCTION

Dye-sensitized solar cells (DSSCs) have attracted great research attention in the past two decades because of their promising cost effectiveness.[1] The total solar-to-electricity conversion efficiency of DSSCs has reached over 12% using n-type semiconductor TiO_2 sensitized with mixed molecular sensitizers.[2] In the past two decades, the vast majority of DSSC works is based on the sensitized photoanodes (the so-called n-DSSCs). Recently, p-type DSSCs based on sensitized photocathodes are attracting increasing attention.[3−8] Studies of p-type DSSCs are mainly motivated to make tandem devices where both electrodes are photoactive, which can overcome the Shockley−Queisser limit to gain higher efficiencies. Moreover these photocathodes can also be used in dye-sensitized photosynthetic cells (DSPSCs) for the production of solar fuels.[9]

Although progress has been made on p-type DSSCs, the study is still in its infancy. Up to now, the most widely studied p-type DSSCs are based on the NiO semiconductor. Another p-type semiconductor such as $CuGaO_2$ has also been recently explored by us and others.[10−13] The efficiencies of NiO DSSCs are still low, suffering from low short-circuit currents (J_{sc}), low open-circuit voltages (V_{oc}), and low fill factors (FFs). The low J_{sc} has been ascribed to the rapid charge recombination between the holes in NiO and the reduced sensitizers.[14−16] A significant percentage of injected holes are lost due to this rapid germinate recombination. Hammarström et al. further found that the ultrafast recombination lies in the Marcus normal region with a large reorganization energy and suspected that the electrons in the reduced sensitizer recombine to the interband states of NiO.[17] To improve the solar cell performance, it is essential to slow down this charge recombination process. A promising approach is to design new push-pull sensitizers that can form long-lived charge-separated states. A carboxylic acid anchoring group is attached to the electron donor part of these push−pull organic sensitizers, and high photon-to-current conversion efficiencies have been achieved.[6−8,18,19] Another approach applied by Odobel and Hammarström et al.[20] is to append an additional electron acceptor to an organic or ruthenium polypyridyl chromophore to achieve the long-lived charge-separated state.[21]

We have been interested in the cyclometalated ruthenium complexes represented as Ru[(N^N)$_2$(C^N)]$^+$ for NiO DSSCs, where N^N represents 2,2′- bipyridine (bpy) and C^N

Received: June 10, 2013
Accepted: August 8, 2013
Published: August 8, 2013

 © 2013 American Chemical Society

Chart 1. Structures of O3, O13, and O17

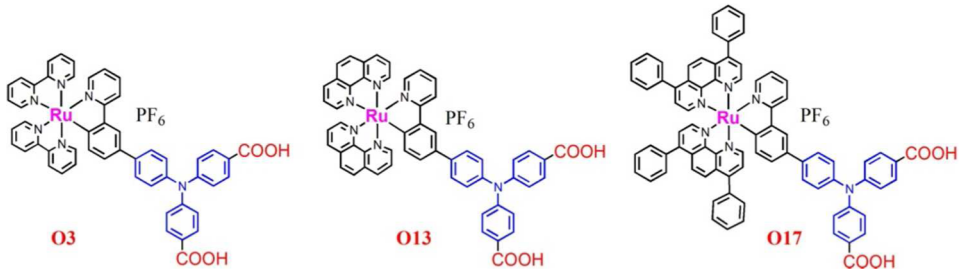

represents bidentate phenylpyridine derivatives. The strong σ-donoting property of the carbon anion in the anionic C^N ligand induces red shift in their absorption spectra. Moreovoer, the HOMO in these complexes is extended to the phenylpyridyl ligand.[22] As a result, the charges in the charge-separated excited states are more spacially separated. In our previous report,[23] we attached the carboxylic acid anchoring group to the anionic C^N ligand for efficient hole injection into NiO and systematically varied the number of phenylene spacer units between the $Ru[(N^{\wedge}N)_2(C^{\wedge}N)]^+$ core and the carboxylic acid anchoring group. We found that the spatial insulation of ruthenium chromophore from the NiO surface is a key to achieving higher photocurrent, which has been attributed to the decreased recombination. The highest J_{sc} obtained is ca. 1.5 mA/cm^2.

In this report, we introduce a triphenylamino (TPA) group to our cyclometalated ruthenium sensitizers as the bridge between the ruthenium chromophore and the NiO surface. The structures are shown in Chart 1. TPA is known as a good hole-conducting unit and has been widely used in molecular designs for a variety of photoelectronic applications.[12,24] Therefore, the TPA bridging group should facilitate the hole transfer from the Ru(II)−N^N core to NiO. In addition, the NN ligand is systematically tuned from 2,2′-bipyridine (**O3**), to 1,10-phenanthroline (**O13**), and to bathophenanthroline (**O17**). Following the series, the conjugation of the N^N ligand is increased, which results in the enhancement of the extinction coefficient. However the solar cell sensitized with **O3** still gives the largest J_{sc} of 3.04 mA/cm^2. The hole transport time and hole lifetime in NiO for these solar cells were studied by intensity-modulated photocurrent spectroscopy (IMPS) and intensity-modulated photovoltage spectroscopy (IMVS), respectively. The results show negligible difference among all the devices, implying that the **O3** solar cell giving the largest J_{sc} is likely caused by its slow geminate charge recombination and efficient dye regeneration.

■ EXPERIMENTAL SECTION

General Information. All reagents and solvents were purchased from Fisher Scientific or Sigma Aldrich Company. The silica gel (60−200 μm) and alumina (60-325 Mesh) for chromatography were also purchased from Fisher Scientific. All products were characterized by ^{1}H NMR (on Bruker) and high-resolution mass spectrometry (HRMS) on a Bruker Daltonics BioTOF system equipped with an electrospray ionization (ESI) source. The absorption spectra were conducted on a PerkinElmer LAMBDA spectrophotometer.

Adsorption Isotherm Measurements. Five solutions of each dye in CH_3CN were prepared. The concentrations range from ∼1 × 10^{-6} to ∼3.9 × 10^{-5} M. NiO films on FTO with an area of 1 cm^2 were immersed into the solutions for 24 h before measurements. After the films were taken out, the UV−vis absorption of the dye solutions was measured. The concentration was calculated by using the molar extinction coeffcient. The difference of concentration before and after the immersion of the films in dye solutions was calcuated to obtain the amount of dye loaded on the films. The dye loading amount was then plotted versus the concentration of dye solution to obtain the adsorption isotherm, which was fitted with a Sips model.

Electrochemistry. Cyclic voltammetry was conducted on a CV50W electrochemical workstation. The three-electrode cell consisted of a Pt working electrode, a Ag/AgCl in saturated KCl as reference electrode, and a Pt wire counter electrode in a single cell compartment. Tetrabutylammonium perchlorate (0.1 M, TBAP) in DMF was used as supporting electrolyte. The scan rate was always 100 mV/s. The ferrocenium−ferrocene ($Fc^{+/0}$) was used as the internal reference, and all potentials were reported relative to NHE using the Fc^+/Fc couple (0.64 V versus NHE) as a reference.

Solar Cell Fabrication and Measurement. $Ni(OH)_2$ sol was prepared following a literature procedure[25,26] by mixing $NiCl_2{\cdot}6H_2O$ and copolymer F108 in the mixture of ethanol and water. NiO film was made by a doctor-blading method with scotch tape on each side of the FTO glass. After drying in air, the film was heated in an oven at 450 °C for 30 min. The film area is aproximately 0.5 × 0.5 cm^2. This doctor-blading and heating procedure was repeated 4 times to achive a thickness of ca. 3 μm measured by an AlphaStep D-100 profilemeter from KLA-Tencor corporation. The films were then soaked in dye solution (0.1−0.2 mM in CH_3CN) for 16 h. After washing with CH_3CN and drying under air, the NiO electrode and platinized counter electrode were sealed by placing and heating a Surlyn 60 film in between. A CH_3CN electrolyte solution consisting of 1.0 M LiI and 0.1 M I_2 was filled through the holes predrilled on the counter electrode by applying vacuum. The holes were sealed afterward with a glass cover slide.

The J−V curves were measured under AM 1.5 solar simulator from PV Measurements and recorded with a CV-50W potentiostat. Intensity-modulated photovoltage (IMVS) and intensity-modulated photocurrent (IMPS) spectra were conducted on Ivium stat from IVIUM technologies under white LED light illumination. The frequency ranges from 100 000 to 0.05 Hz. The hole transport time and lifetime are calculated by $1/2\pi f_{max}$. The f_{max} is the frequency where maximum inductance (for τ_{tr}) and impedance (for τ_h) are obtained in Bode plots.

Density Functional Theory Calculations. All computations were carried out with the Gaussian 09[27] software package at the Ohio supercomputer center. All ground-state structures were optimized by using density functional theory (DFT) with the B3LYP function[28,29] for C, H, O, and N and with the LanL2DZ basis[30] set for the ruthenium atom. A single-point energy calculation was carried on the optimized structure to obtain the Mulliken population analysis and the contributions to the frontier molecular orbitals from different functional groups divided into triphenylamino ligand (TPA), N^N ligand (N^N), N^C ligand (N^C), and ruthenium metal center (Ru). Time-dependent density functional theory (TD-DFT) calculations were performed based on the optimized ground-state structures with spin restriction using the B3LYP functional for C, H, O, and N and with the LanL2DZ basis set for ruthenium to obtain the excitations. The excitation spectra were obtained using GaussSum software.

Scheme 1. Synthetic Route of O3

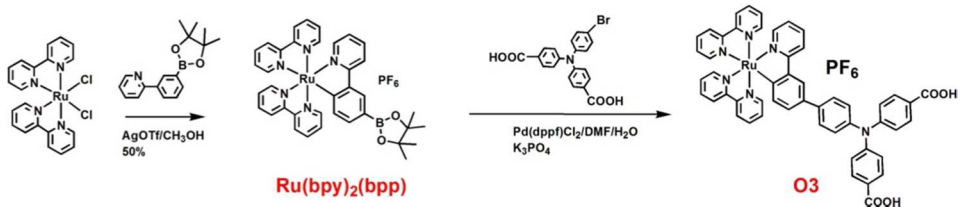

Scheme 2. Synthetic Route of O13 and O17

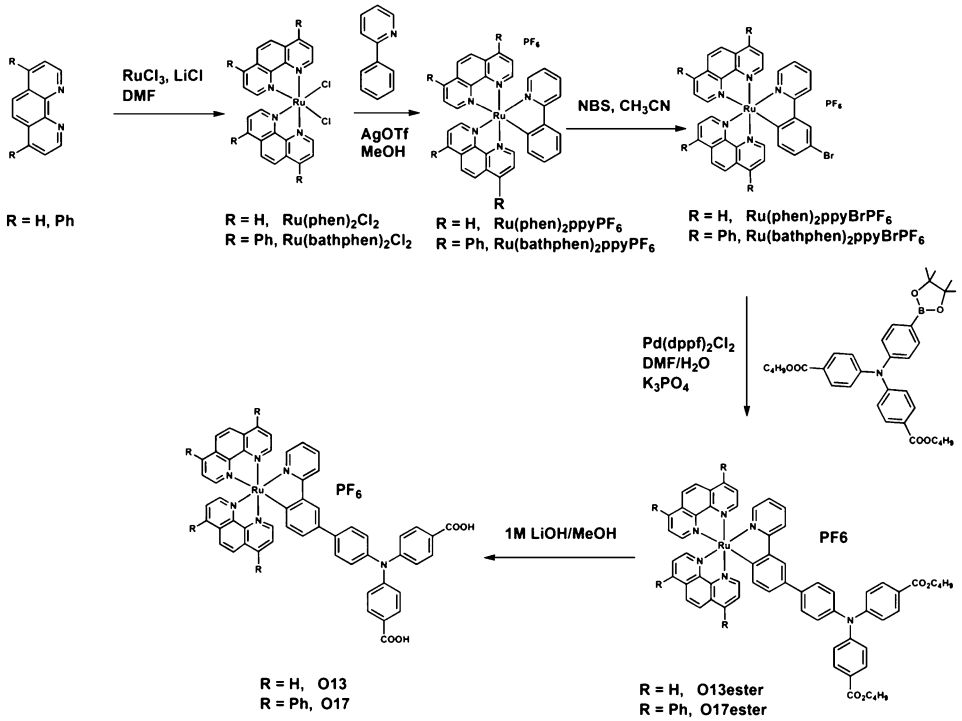

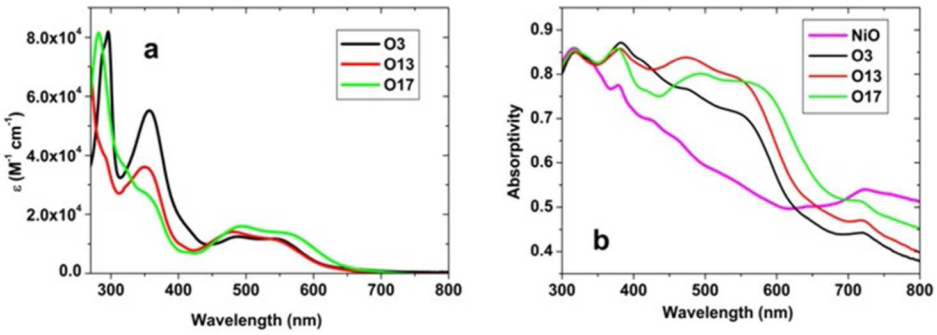

Figure 1. (a) Absorption spectra of O3, O13, and O17 in DMF solutions. (b) The absorption spectra of NiO, O3/NiO, O13/NiO, and O17/NiO films.

■ RESULTS AND DISCUSSION

Synthesis. Two methods were applied to synthesize the sensitizers. The synthetic routes are depicted in Scheme 1 and Scheme 2. In the first method, following our previous procedure,[23] a one-step Suzuki coupling between $Ru(bpy)_2bpp$ and *N*,*N*-di(carboxylate)-4-bromo-phenylamine was employed to synthesize O3. To synthesize O13 and O17, Ru-[N^N]$_2$[C^N], where N^N represents 1,10-phenanthroline (O13) or bathophenanthroline (O17) and C^N represents 2-phenylpyridine, was prepared by modification of literature procedure.[31] In the presence of NBS in CH_3CN, Ru-[N^N]$_2$[C^N] was brominated exclusively at the -para position to the ruthenium−carbon bond.[32] The high regioselectivity has been correlated to the high electron density at this position. A subsequent Suzuki coupling reaction with *N*,*N*-di(4-benzoic acid *tert*-butyl ester)-4-(4,4,5,5-tetramethyl-[1,3,2]-dioxaborolan-2-yl)-phenylamine[33] in the presence of Pd(dppf)-Cl_2 and 1 M aq. K_3PO_4 gave the *tert*-butyl ester protected complexes, which were subsequently removed in methanolic

Table 1. Photophysical and Electrochemical Data of O3, O13, and O17

	λ/nm (ε/M^{-1} cm^{-1})	E_{ox} (V)	E_{red} (V)	E_{00} (eV)[a]	$E^{*/-1}$ (V)
O3	483 (12390), 543 (11830)	0.59, 1.13	−1.49, −1.78	1.95	0.46
O13	484 (14070), 538(11673)	0.50, 1.04	−1.35	1.90	0.55
O17	494 (16020), 559 (13680)	0.56, 1.08	−1.24, −1.46	1.70	0.46

[a] E_{00} is estimated from the on-site of the absorption spectrum.

LiOH in high yields. All sensitizers were characterized by ^{1}H NMR and ESI−MS.

Electronic Absorption. All absorption spectra taken in DMF solutions are displayed in Figure 1a. All sensitizers exhibit broad absorption spectra including the UV region from 250 to ca. 400 nm assigned as π−π^* transitions and from 400 to ca. 700 nm with molar absorption coefficients of ∼1 × 10^4 M^{-1} cm^{-1}, assigned as spin-allowed ^{1}MLCT transitions. The absorption maxima and the molar absorption coefficients beyond 400 nm of all sensitizers are summarized in Table 1. The spectrum of O17 red shifts by around ∼20 nm compared to O3 and O13. In addition, the molar absorption coefficient slightly increases from O3, to O13, and to O17 from 1.1 × 10^4 to 1.4 × 10^4 M^{-1} cm^{-1} due to the incorporation of the expanded π conjugation ligand.

The absorption spectra of sensitized films and a bare NiO film are shown in Figure 1b. The thickness of the films is ∼2 μm. The absorption maxima and the corresponding absorptivity (showing in parentheses) are 481 (0.76) and 558 (0.70) for O3, 476 (0.84) and 548 (0.79) for O13, and 497(0.80) and 566 (0.78) for O17, respectively. The absorption spectra of sensitized films are consistent with the solution spectra with changes within less than 15 nm, suggesting there is no ground-state electronic structure change or aggregation when the sensitizers are chemically adsorbed on NiO film. It is noteworthy that bare NiO film absorbed part of the light (ca. 50% at 600 nm and 60% at 480 nm), showing a dark brown color. By integrating the absorption spectra from 300 to 700 nm for all sensitized films, the absorption of sensitized films toward input light source can be estimated. The results show that the light harvesting ability of O13 and O17 films increases by 5.6% and 7.8% compared to the O3 film.

Adsorption of Sensitizers on NiO Films. The adsorption of sensitizers on NiO films was performed to quantify the amount of dye loading. The adsorption isotherms by plotting the amount of surface-loaded dyes on NiO films versus the concentration of dye solutions are shown in Figure 2. A Sips model[34,35] was applied to best fit our data, possibly due to the heterogeneous surface of NiO and the interaction between the sensitizers on NiO films. The same model has been previously used by us to model the adsorption of organic sensitizers on NiO films.[36] The model describes the dependence of surface loading q on the solution concentration c as

$$q = q_m \frac{(K_c c)^b}{1 + (K_c c)^b}$$

where q_m is the maximum amount of surface loading; K_c is the binding constant; and b is indicative of the surface heterogeneity of NiO surface. All fitting parameters are included in Table 2. The results show that all sensitizers exhibit a similar surface loading behavior including comparable surface binding constants and maximum amounts of surface loading. The maximum surface loading of O3, O13, and O17 is 33.13, 31.7, and 33.3 nanomol/cm^2, respectively. The results indicate that any difference of the performance of the solar cell devices should not stem from the adsorption of sensitizers on the NiO surface.

Table 2. Parameters from the Sips Fittings of Adsorption Isotherms of O3, O13, and O17 on NiO Films

	O3	O13	O17
q_m (nmol/cm^2)	33.1 ± 0.23	31.7 ± 0.23	33.3 ± 1.07
K_c (10^5 M)	3.81 ± 0.05	3.34 ± 0.04	2.94 ± 0.20
b	1.83 ± 0.05	2.69 ± 0.09	1.96 ± 0.23
R^2	0.999	0.999	0.996

Electrochemistry. The cyclic voltammograms (CVs) of the three sensitizers were measured in dry DMF solutions with 0.1 M TBAP supporting electrolyte. All potentials are reported versus NHE with data shown in Table 1. The redox potentials together with VB of NiO and redox potential of electrolyte is schematically shown in Figure 3. All sensitizers exhibit two reversible oxidation potentials at 0.59 and 1.13 V for O3, 0.50 and 1.04 V for O13, and 0.56 and 1.08 V for O17. The first oxidation potential is assigned as Ru(III)/(II), and the second oxidation potential is in line with the oxidation potential of triphenylamino groups.[6,19] These assignments are also consistent with our DFT calculations (vide infra). The

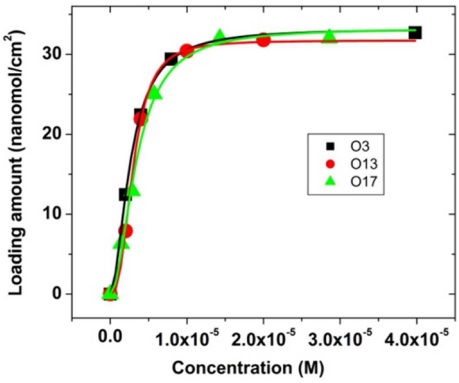

Figure 2. Adsorption isotherms of O3, O13, and O17 on NiO films and the fittings with a Sips model.

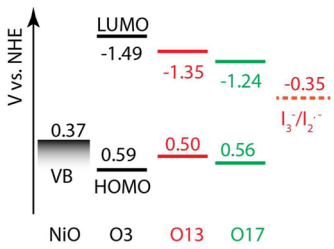

Figure 3. Schematic of redox potentials of all sensitizers, redox couple, and VB of the NiO semiconductor.

oxidation potential of Ru(III)/(II) for all sensitizers is at a similar level with differences less than 90 mV. The reduction potential is assigned as one-electron and two-electron reduction of N^N ligands. As can be seen, the first reduction potential exhibits positive shift away from vacuum from O3, to O13, to O17 by 250 mV owing to the enhanced π conjugation, which is consistent with the observed absorption spectra. The excited state reduction potential can be calculated from the following equation: $E^{*/-} = E_{00} + E^{0/-}$ as 0.46, 0.55, and 0.46 V (vs NHE) for O3, O13, and O17, respectively. The flat band potential of NiO prepared in our lab was determined as 0.37 Vs NHE by photoelectrochemical methods. Therefore the hole injection from the excited sensitizers to VB of NiO is thermodynamically favorable.

DFT and TDDFT Calculations. DFT calculations were performed to optimize the ground-state structures by using the LANL2DZ basis set for the ruthenium atom. TD-DFT on optimized structures in CH_3CN by using the PCBM solvation field built in Gaussian 09 software were used to obtain the electronic absorption spectra and energy levels. The molecular orbital composition analysis was done by using GaussSum software. All sensitizers exhibit similar molecular orbital components. O3 is shown in Table 3 as a representative and discussed in detail. The calucation results of O13 and O17 are shown in Tables S1 and S2 (Supporting Information). The molecule was mandatorily divided into four different functional groups including the triphenylamino ligand (TPA), the N^N ligand (N^N), the N^C ligand (N^C), and the ruthenium metal center (Ru). The results reveal the delocalization of HOMO onto the N^C ligand with 67% on the ruthenium center and 20% on the phenylpyridyl ligand. It is noteworthy that 6% of HOMO is localized on TPA, which may facilitate the hole injection. The result is also consistent with the first oxidation potential being assigned as Ru(III)/(II). 97% of the LUMO orbital is localized on N^N, and 93% of LUMO+1 is localized on N^C.

Table 3. Molecular Orbital Composition Analysis of O3 in a CH_3CN Continuum (All Are Shown in Percentage)

O3	Ru	N^C	N^N	TPA
HOMO	67	20	6	6
HOMO-1	80	6	13	0
HOMO-2	10	82	7	1
LUMO	2	1	97	0
LUMO+1	6	93	0	0
LUMO+2	0	0	0	100

The simulated absorption spectra obtained by TD-DFT calculations (shown in Figure S1, Supporting Information) exhibit a blue shift by ca. 50 nm relative to the experimental data; however, similar trends are observed. From O3, to O13, and to O17, the simulated molar absorption coefficient increases, revealing superior light harvesting capability. The frontier orbital energy levels and the isodensity plots of HOMO and LUMO of all sensitizers are shown in Figure 4. Consistent with electrochemical results, the calculated HOMO level remains relatively unchanged; however, the LUMO energy level decreases (away from vacuum) across the series causing the driving force for charge recombination to decrease.

Tables S3−S5 (Supporting Information) show major spin-allowed transitions and the major orbital contributions to these transitions. In the case of O3, the lowest energy transition at 531 nm with oscillation strength of 0.02 mainly involves HOMO-2 to LUMO+1 (55%) and HOMO-2 to LUMO (18%) and the transition at 488 nm with oscillation strength of 0.098 involves HOMO-2 to LUMO (40%) and HOMO-2 to LUMO +1 (28%). The results indicate that the principal contribution to the lower energy band is mainly charge transfer transitions and metal perturbed intraligand transitions from the ruthenium metal center with contribution of the N^C ligand to either the N^N or N^C ligand. The N^N and N^C ligands are close in energy, resulting in multiple transitions that account for the broad absorption spectra of these cyclometalated ruthenium complexes.[22]

Performance and Characterization of Solar Cell Devices. Solar cells were made by following our previous reports consisting of ∼2 μm thick nanoporous NiO films sensitized with sensitizers, a CH_3CN electrolyte of 1.0 M LiI and 0.1 M I_2, and a platinized counter electrode.[23] The performance of all devices was measured under an AM 1.5G solar simulator. The $J-V$ characteristic curves of all solar cells are shown in Figure 5 with all parameters summarized in Table 4. Our best solar cell is achieved by using O3 as the sensitizer to give a J_{sc} of 3.04 mA/cm^2, V_{oc} of 93 mV, and efficiency of 0.099%. Such a photocurrent is significantly larger than our prior cyclometalated ruthenium dyes with phenylene links.[23]

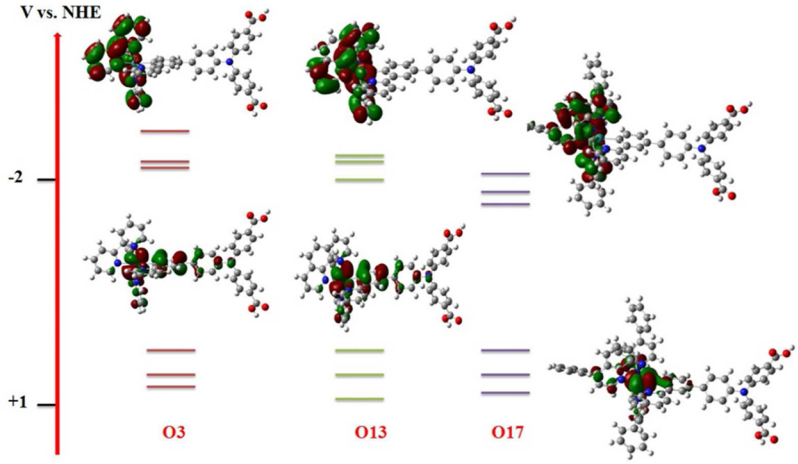

Figure 4. Isodensity plots of HOMO and LUMO and the energy levels of the frontier orbitals obtained by TD-DFT calculations.

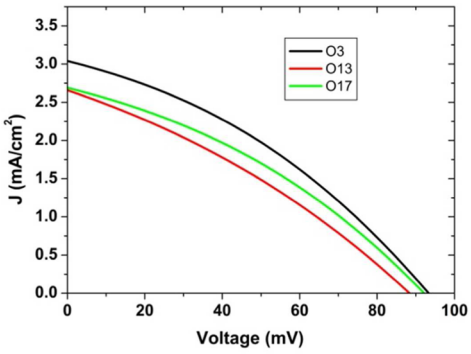

Figure 5. $J-V$ characteristic curves of O3, O13, and O17 solar cells.

Table 4. Solar Cell Parameters of All Devices

	J_{sc} (mA/cm^2)	V_{oc} (mV)	FF (%)	η (%)
O3	3.04	93	0.35	0.099
O13	2.66	89	0.31	0.074
O17	2.69	92	0.34	0.085

The IPCE spectra of all cells were measured. The results are shown in Figure S2 (Supporting Information). The comparison with the corresponding absorption spectra confirms that the photocurrent is generated by the absorption of the cyclometalated ruthenium sensitizers.

While all solar cells give similar V_{oc} values, the J_{sc} decreases from O3 to O13 and O17 by 12.5% and 11.5%, respectively, despite the increased light harvesting efficiency (LHE) by 5.6% and 7.8% calculated from the absorption measurement. In a DSSC device, The short-circuit current is an integration of incident photon to current conversion efficiency (IPCE) over the solar spectrum, which is determined by the following equation

$$\mathrm{IPCE} = \mathrm{LHE} \times \eta_{inj} \times \eta_{col} \times \eta_{reg}$$

where LHE is the light harvesting efficiency determined by the absorption of the film; η_{inj} is the injection efficiency; η_{col} is the hole collection efficiency; and η_{reg} is the dye regeneration efficiency.

Unlike TiO_2 solar cells where η_{reg} is usually unity, dye regeneration in a p-type DSSC cannot be neglected, due to the fast charge recombination. In fact, Gibson et al.[37] found inefficient regeneration of the sensitizer appears to be the efficiency-limiting step in the device using a series of perylene imide sensitizers. In the case of our sensitizers, the only structural change is the N^N ligand, which imposes less structure and electronic effect on the oxidation potential (see Electrochemistry section). All ruthenium chromophores are anchored through the triphenylamino group. The electronic coupling for hole injection is expected to be similar, therefore it is reasonable to assume that all sensitizers should have comparable hole injection efficiency (η_{inj}). Thus, the higher short-circuit current density observed for the O3 solar cell can be the result of either better charge collection efficiency or more efficient dye regeneration.

To investigate the charge collection efficiency of solar cells, the hole transport and recombination kinetics were studied by intensity-modulated photocurrent spectroscopy (IMPS) and intensity-modulated photovoltage spectroscopy (IMVS). Both techniques are frequency domain techniques, which measure the response of photocurrent or voltage to a small perturbation of light intensity.[38] IMPS measures the response of current as the function of a modulation of light intensity at the short-circuit condition. Figure 6a shows the hole transport time (τ_{tr}) plotted versus the short-circuit current. In contrary to TiO_2 solar cells for which electron transport time is an exponential function of light intensity, the hole transport times are invariant at lower light intensity but decrease sharply at higher light intensity. This phenomenon has been reported for NiO DSSCs in the literature.[20,39] The reason is unclear, but Zhu et al. suggest a hole hopping mechanism to explain their results.[39] The τ_{tr} of all devices is similar in range from 63 to 73 ms at short-circuit current lower than ~1 mA/cm^2. The hole transport coefficient, D, therefore can be calculated from the equation[5,26]

$$D = \frac{d^2}{2.77\tau_{tr}}$$

where d is the film thickness. The thickness of our film is ~2 μm, and the average τ_{tr} is taken as 70 ms. Then the hole transport coefficient of our NiO film is calculated to be 2.1×10^{-7} cm^2 s^{-1}, similar to the reported values.[26,39,40]

IMVS is performed at the open-circuit condition by a small modulation of light intensity. The hole lifetime (τ_h) is plotted versus open-circuit voltage in Figure 6b. The τ_h is an exponential function of the open-circuit voltage of devices by adjusting light intensity and exhibits negligible difference among the devices. Hole collection efficiency therefore can be calculated by the equation

$$\eta_{col} = 1 - \frac{\tau_{tr}}{\tau_h}$$

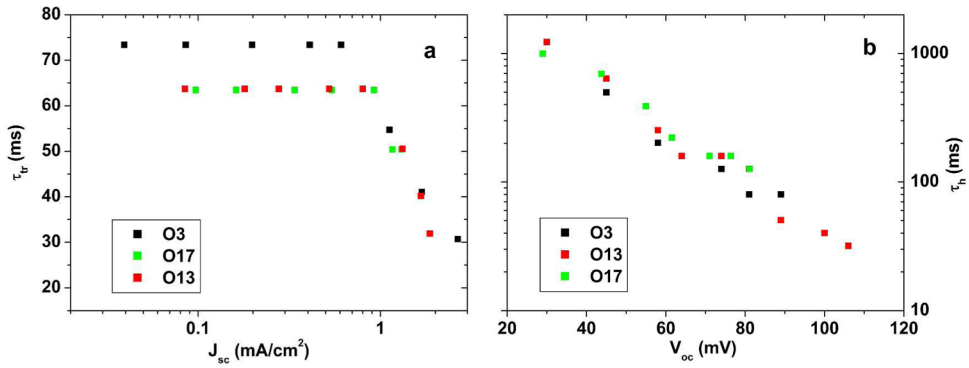

Figure 6. (a) Hole transport time (τ_{tr}) as a function of J_{sc} and (b) hole lifetime (τ_h) as a function of V_{oc}.

The charge collection efficiency varies with light intensity. At low light intensity, η_{col} of our solar cells is calculated as high as 98%. In addition, as can be seen, there is only a negligible difference of hole collection efficiency among all devices.

The small difference of charge collection efficiency among all the solar cells made of three sensitizers is unlikely to be the cause of the different J_{sc}. However, it is important to note that IMVS is performed in the frequency range of 100 000 to 0.05 Hz, which corresponds to a time range of 1.6 μs to 3.2 s. Any electron transfer process faster than this time domain cannot be measured by this technique. Similar lifetimes of holes among all devices obtained at this relatively long time domain mainly suggest that the back electron transfer of holes in NiO films to the electrolyte is unchanged with respect to different sensitizers.

On the other hand, another important factor usually determining the current output of a DSSC device is the fast germinate charge recombination between holes on NiO and electrons on the reduced sensitizers. In this circumstance, the lifetime of the reduced sensitizers on NiO films after photoillumination is related to the performance of solar cell devices. For NiO DSSCs, the fast germinate charge recombination is known to be deleterious to the device performance. Previously the ultrafast geminate charge recombination occurring in the picosecond−nanosecond time domain has been observed, when coumarins, porphyrin, and naphthaline were used as sensitizers.[15,16,41] The longer lifetime of the reduced sensitizer provides larger chance for photogenerated holes to be collected by an external circuit, thus larger current density, and larger opportunities for the sensitizers to be regenerated. In a recent report, we found that the charge recombination in our cyclometalated ruthenium-sensitized NiO films occurred in the picosecond scale, and we postulate that this is due to the low hole mobility and small dielectric constant of NiO.[23] In this study, the only structural change of the sensitizers is the N^N ligand, which imposes the most significant effect on the reduction potential and consequently the driving force for electron−hole pair recombination. Furthermore, as we discussed, the dye regeneration efficiency of the NiO DSSC is usually not unity. It has been generally accepted that in a NiO DSSC the reduced dye is regenerated by $I_3^-/I_2^{\bullet-}$ with its redox potential at approximately −0.35 V vs NHE.[20,42,43] Following the series, O3 has the largest driving force for dye regeneration, which might be another explanation for its best performance.

Our collective results indicate that, following the series, as the conjugation of the N^N ligand is increased the light harvesting capability of the sensitizer is enhanced. The largest J_{sc}, however, is achieved when O3 is used as the sensitizer. Such results suggest that, for O3, the larger J_{sc} is likely caused by the slow geminate charge recombination. This longer lived interfacial charge-separated state provides more opportunity for the reduced O3 to be regenerated by I_3^- in the electrolyte. The results imply that the auxilary N^N ligands play a very important role in the eletron−hole recombination kinetics and thus the device performance.

■ CONCLUSIONS

We have reported three new cyclometalated ruthenium sensitizers with a triphenylamino group as a linker to bridge the ruthenium chromophore to the NiO surface. A J_{sc} of 3.04 mA/cm^2 has been obtained for solar cell devices sensitized with O3, which is close to the largest J_{sc} reported in the literature.[7,19] The results highlight the promising potential of using cyclometalated ruthenium sensitizers for NiO DSSCs. In addition, the performance of devices and electron transfer at the sensitizer/NiO interface has been systematically studied by IMPS and IMVS. The collective results suggest that the O3 solar cell giving the largest J_{sc} is likely caused by the slow geminate charge recombination and efficient dye regeneration.

■ ASSOCIATED CONTENT

Ⓢ Supporting Information

Detailed synthetic route and characterization of synthesized sensitizers and additional DFT and TD-DFT calculation results. This material is available free of charge via the Internet at http://pubs.acs.org.

■ AUTHOR INFORMATION

Corresponding Author

*E-mail: wu@chemistry.ohio-state.edu.

Notes

The authors declare no competing financial interest.

■ ACKNOWLEDGMENTS

This work was supported by the U.S. Department of Energy, Office of Basic Energy Sciences, Division of Materials Science and Engineering under Award DE-FG02-07ER46427.

■ REFERENCES

(1) O'Regan, B.; Grätzel, M. *Nature* **1991**, *353* (6346), 737−40.
(2) Yella, A.; Lee, H.; Tsao, H.; Yi, C.; Chandiran, A.; Nazeeruddin, M.; Diau, E.; Yeh, C.; Zakeeruddin, S.; Grätzel, M. *Science* **2011**, *334*, 629−634.
(3) He, J.; Lindström, H.; Hagfeldt, A.; Lindquist, S.-E. *J. Phys. Chem. B* **1999**, *103* (42), 8940−8943.
(4) Odobel, F.; Le Pleux, L.; Pellegrin, Y.; Blart, E. *Acc. Chem. Res.* **2010**, *43* (8), 1063−1071.
(5) Odobel, F.; Pellegrin, Y.; Gibson, E. A.; Hagfeldt, A.; Smeigh, A.; Hammarström, L. *Coord. Chem. Rev.* **2012**, *256* (21−22), 2414−2423.
(6) Qin, P.; Zhu, H.; Edvinsson, T.; Boschloo, G.; Hagfeldt, A.; Sun, L. *J. Am. Chem. Soc.* **2008**, *130* (27), 8570−8571.
(7) Nattestad, A.; Mozer, A. J.; Fischer, M. K. R.; Cheng, Y. B.; Mishra, A.; Baeuerle, P.; Bach, U. *Nat. Mater.* **2009**, *9* (1), 31−35.
(8) Ji, Z.; Natu, G.; Huang, Z.; Wu, Y. *Energy Environ. Sci.* **2011**, *4*, 2818−2821.
(9) Li, L.; Duan, L.; Wen, F.; Li, C.-Y.; Wang, M.; Hagfeldt, A.; Sun, L. *Chem. Commun.* **2012**, *48*, 988−990.
(10) Yu, M.; Natu, G.; Ji, Z.; Wu, Y. *J. Phys. Chem. Lett.* **2012**, *3*, 1074−1078.
(11) Renaud, A.; Chavillon, B.; Le Pleux, L.; Pellegrin, Y.; Blart, E.; Boujtita, M.; Pauporte, T.; Cario, L.; Jobic, S.; Odobel, F. *J. Mater. Chem.* **2012**, *22*, 14353−14356.
(12) Bai, J.; Xu, X.; Xu, L.; Cui, J.; Huang, D.; Chen, W.; Cheng, Y.; Shen, Y.; Wang, M. *ChemSusChem* **2013**, *6* (4), 622−629.
(13) Xiong, D.; Xu, Z.; Zeng, X.; Zhang, W.; Chen, W.; Xu, X.; Wang, M.; Cheng, Y. *J. Mater. Chem.* **2012**, *22* (47), 24760−24768.
(14) Borgstrom, M.; Blart, E.; Boschloo, G.; Mukhtar, E.; Hagfeldt, A.; Hammarström, L.; Odobel, F. *J. Phys. Chem. B* **2005**, *109* (48), 22928−34.
(15) Morandeira, A.; Boschloo, G.; Hagfeldt, A.; Hammarström, L. *J. Phys. Chem. B* **2005**, *109* (41), 19403−10.
(16) Morandeira, A.; Boschloo, G.; Hagfeldt, A.; Hammarström, L. *J. Phys. Chem. C* **2008**, *112* (25), 9530−9537.
(17) Smeigh, A.; Le Pleux, L.; Fortage, J.; Pellegrin, Y.; Blart, E.; Odobel, F.; Hammarstrom, L. *Chem. Commun.* **2012**, *48*, 678−680.
(18) Li, R.; Lv, X.; Shi, D.; Zhou, D.; Cheng, Y.; Zhang, G.; Wang, P. *J. Phys. Chem. C* **2009**, *113*, 7469−7479.
(19) Qin, P.; Linder, M.; Brinck, T.; Boschloo, G.; Hagfeldt, A.; Sun, L. *Adv. Mater.* **2009**, *21* (29), 2993−2996.

(20) Le Pleux, L.; Smeigh, A. L.; Gibson, E. A.; Pellegrin, Y.; Blart, E.; Boschloo, G.; Hagfeldt, A.; Hammarstroem, L.; Odobel, F. *Energy Environ. Sci.* **2011**, *4*, 2075−2084.
(21) Freys, J.; Gardner, J.; D'Amario, L.; Brown, A.; Hammarström, L. *Dalton Trans.* **2012**, *41*, 13105−13111.
(22) Bomben, P. G.; Robson, K. C. D.; Sedach, P. A.; Berlinguette, C. P. *Inorg. Chem.* **2009**, *48* (20), 9631−9643.
(23) Ji, Z.; Natu, G.; Huang, Z.; Kokhan, O.; Zhang, X.; Wu, Y. *J. Phys. Chem. C* **2012**, *116* (32), 16854−16863.
(24) Thomas, K.; Velusamy, M.; Lin, J. T.; Chuen, C.; Tao, Y. *J. Mater. Chem.* **2005**, *15*, 4453−4459.
(25) Sumikura, S.; Mori, S.; Shimizu, S.; Usami, H.; Suzuki, E. *J. Photochem. Photobiol. A* **2008**, *199*, 1−7.
(26) Li, L.; Gibson, E. A.; Qin, P.; Boschloo, G.; Gorlov, M.; Hagfeldt, A.; Sun, L. *Adv. Mater.* **2010**, *22* (15), 1759−1762.
(27) Gaussian 03, Frisch, M. J.; Trucks, G. W.; Schlegel, H. B.; Scuseria, G. E.; Robb, M. A.; Cheeseman, J. R.; Montgomery, J. A., Jr.; Vreven, T.; Kudin, K. N.; Burant, J. C.; Millam, J. M.; Iyengar, S. S.; Tomasi, J.; Barone, V.; Mennucci, B.; Cossi, M.; Scalmani, G.; Rega, N.; Petersson, G. A.; Nakatsuji, H.; Hada, M.; Ehara, M.; Toyota, K.; Fukuda, R.; Hasegawa, J.; Ishida, M.; Nakajima, T.; Honda, Y.; Kitao, O.; Nakai, H.; Klene, M.; Li, X.; Knox, J. E.; Hratchian, H. P.; Cross, J. B.; Bakken, V.; Adamo, C.; Jaramillo, J.; Gomperts, R.; Stratmann, R. E.; Yazyev, O.; Austin, A. J.; Cammi, R.; Pomelli, C.; Ochterski, J. W.; Ayala, P. Y.; Morokuma, K.; Voth, G. A.; Salvador, P.; Dannenberg, J. J.; Zakrzewski, V. G.; Dapprich, S.; Daniels, A. D.; Strain, M. C.; Farkas, O.; Malick, D. K.; Rabuck, A. D.; Raghavachari, K.; Foresman, J. B.; Ortiz, J. V.; Cui, Q.; Baboul, A. G.; Clifford, S.; Cioslowski, J.; Stefanov, B. B.; Liu, G.; Liashenko, A.; Piskorz, P.; Komaromi, I.; Martin, R. L.; Fox, D. J.; Keith, T.; Al-Laham, M. A.; Peng, C. Y.; Nanayakkara, A.; Challacombe, M.; Gill, P. M. W.; Johnson, B.; Chen, W.; Wong, M. W.; Gonzalez, C.; Pople, J. A. *Gaussian 03*; Gaussian, Inc.: Wallingford, CT, 2004.
(28) Lee, C.; Yang, W.; Parr, P. G. *Phys. Rev. B* **1988**, *37*, 785−789.
(29) Becke, A. D. *J. Chem. Phys.* **1993**, *98*, 5648−5652.
(30) Hay, P. J.; Wadt, W. R. *J. Chem. Phys.* **1985**, *82*, 299−310.
(31) Sasaki, I.; Vendier, L.; Sournia-Saquet, A.; Lacroix, P. G. *Eur. J. Inorg. Chem.* **2006**, *16*, 3294−3302.
(32) Collin, J.; Kayhanian, R.; Sauvage, J.; Calogero, G.; Barigelletti, F.; De Cian, A.; Fischer, J. *Chem. Commun.* **1997**, 775−776.
(33) Chang, C.-H.; Chen, Y.-C.; Hsu, C.-Y.; Chou, H.-H.; Lin, J. T. *Org. Lett.* **2012**, *14* (18), 4726−4729.
(34) Sips, R. *J. Chem. Phys.* **1948**, *16*, 490−495.
(35) Sips, R. *J. Chem. Phys.* **1950**, *18*, 1024−1026.
(36) Natu, G.; Huang, Z.; Ji, Z.; Wu, Y. *Langmuir* **2012**, *28* (1), 950−956.
(37) Gibson, E. A.; Le Pleux, L.; Fortage, J.; Pellegrin, Y.; Blart, E.; Odobel, F.; Hagfeldt, A.; Boschloo, G. *Langmuir* **2012**, *28*, 6485−6493.
(38) Frank, A. J.; Kopidakis, N.; Van de Lagemaat, J. *Coord. Chem. Rev.* **2004**, *248* (13−14), 1165−1179.
(39) Zhu, H.; Hagfeldt, A.; Boschloo, G. *J. Phys. Chem. C* **2007**, *111* (47), 17455−17458.
(40) Sumikura, S.; Mori, S.; Shimizu, S.; Usami, H.; Suzuki, E. *J. Photochem. Photobiol., A* **2008**, *199* (1), 1−7.
(41) Morandeira, A.; Fortage, J.; Edvinsson, T.; Le Pleux, L.; Blart, E.; Boschloo, G.; Hagfeldt, A.; Hammarström, L.; Odobel, F. *J. Phys. Chem. C* **2008**, *112* (5), 1721−1728.
(42) Boschloo, G.; Hagfeld, A. *Acc. Chem. Res.* **2009**, *42*, 1819−1826.
(43) Qin, P.; Wiberg, J.; Gibson, E. A.; Linder, M.; Li, L.; Brinck, T.; Hagfeldt, A.; Albinsson, B.; Sun, L. *J. Phys. Chem. C* **2010**, *114* (10), 4738−4748.